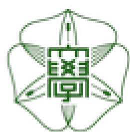
HOKKAIDO UNIVERSITY

Title	High-repetition-rate (6 kHz) and long-pulse-duration (50 ns) ArF excimer laser for sub-65 nm lithography
Author(s)	Kakizaki, Koji; Sasaki, Yoichi; Inoue, Toyoharu; Sakai, Yosuke
Citation	Review of Scientific Instruments, 77(3), 035109-1-035109-6 https://doi.org/10.1063/1.2182744
Issue Date	2006-03
Doc URL	http://hdl.handle.net/2115/8471
Rights	Copyright © 2006 American Institute of Physics
Type	article
File Information	RSI_77_035109.pdf

Instructions for use

Hokkaido University Collection of Scholarly and Academic Papers : HUSCAP

High-repetition-rate (6 kHz) and long-pulse-duration (50 ns) ArF excimer laser for sub-65 nm lithography

Koji Kakizaki, Yoichi Sasaki, and Toyoharu Inoue
Ushio Inc., 400 Yokokurashinden, Oyama, Tochigi 323-8558, Japan

Yosuke Sakai
Hokkaidou University, North 13, West 8, Sapporo, Hokkaido 060-0814, Japan

(Received 2 July 2005; accepted 5 February 2006; published online 22 March 2006)

Development of high-repetition-rate ArF excimer lasers is vital requirement for achieving high throughput and high energy-dose stability in a scanner system. ArF excimer laser, with increasing light pulse duration, can reduce the peak power without the energy-dose change. Then, the spectral bandwidth $\Delta\lambda_{FWHM}$ becomes narrower by increasing the number of light round trips in a cavity, and optical damage is reduced from high-peak power. Laser operation exceeding 4 kHz is needed for next-generation technologies that can enable high numerical aperture and development of high-throughput scanners. In the present work, we examined the possibilities of achieving a repetition rate to 6 kHz from 4 kHz in the ArF laser the authors developed, taking the following innovations. The spatial width of discharge region was reduced by about 30%. The uniform gas flow condition between the electrodes was obtained by improving gas flow guides. As a result, we have obtained an average power of 42 W, a standard deviation for pulse-to-pulse energy of 3.5%, and an integral-square pulse width T_{is} of 44 ns at 6 kHz for $\Delta\lambda_{FWHM} < 0.40$ pm. Finally, it was concluded that developing a 6 kHz ArF excimer laser for the next-generation sub-65 nm lithography is feasible. © *2006 American Institute of Physics.* [DOI: 10.1063/1.2182744]

I. INTRODUCTION

During the last decade, much progress in ArF excimer lithography has been made as a result of a joint effort of semiconductor manufacturers and their process equipment makers. Device mass production through ArF excimer lithography has started from its target node of 90 nm (half pitch). Recently the long-term stability of over 10×10^9 pulses in a 4 kHz ArF excimer laser is achieved.[1] In our previous work, we developed a narrow-spectral-bandwidth 4 kHz ArF excimer laser.[2] The main feature of this laser was the oscillation of long laser pulse duration with low-peak power: consequently the narrow-spectral-bandwidth laser light was obtained by increasing the number of round trips of laser light between the cavity mirrors, and the optical damage was reduced.

The laser performances we are seeking in response to demands in the new generation of stepper/scanner technology, e.g., high numerical aperture (NA), high-throughput scanners, etc., are summarized in Table I. To optimize laser for next-generation technologies with sub-65 nm node design rules, we have to develop ArF laser with performances of not only narrower spectral bandwidths but also higher operating rates that exceed 4 kHz. So far, though ArF excimer lasers with over 4 kHz operation have been described, a narrow-bandwidth 6 kHz ArF excimer laser has not been obtained.[3–5]

In the present article, we report a next-generation ArF excimer laser with a repetition rate of 6 kHz. This laser was reconstructed using a prototype 4 kHz excimer laser designed to analyze the possibilities of achieving higher-repetition-rate operation. We focused to examine on the pulse-to-pulse energy stability and the laser pulse width extension. Their qualities degrade appreciably due to descent of discharge stability at high-repetition-rate operation. Next, we examine laser output characteristics for a repetition rate of 6 kHz.

II. LASER SYSTEM

A. Improvement of 4 kHz ArF laser to 6 kHz operation mode

Figure 1 shows a schematic diagram of a 6 kHz ArF excimer laser system. This system consists of a laser chamber (discharge circuit, main discharge electrodes, preionizer, fan, and laser gas), a pulse power module (switching unit,

TABLE I. Relation between stepper/scanner characteristics and laser performance.

Stepper/scanner characteristics	Laser performance
High NA	Narrow bandwidth Wavelength stability
High throughput	High-average power High repetition rate
High critical dimension control	Energy stability High repetition rate Wavelength stability
Low operating cost	Long lifetime High durability

 © 2006 American Institute of Physics

Downloaded 08 May 2006 to 133.50.98.38. Redistribution subject to AIP license or copyright, see http://rsi.aip.org/rsi/copyright.jsp

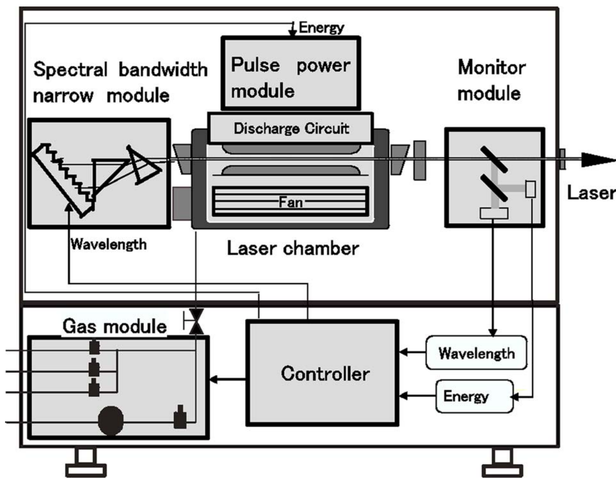

FIG. 1. ArF excimer laser system.

magnetic pulse compression circuit, and charger), a spectral bandwidth narrow module, a monitor module to detect the optical performance of the laser beam, a gas module to supply to and exhaust from the chamber, and a controller of each module. We developed the 6 kHz ArF excimer laser introducing the following new devices.

1. Laser chamber

A high-efficiency discharge circuit. The floating inductance of the discharge-current circuit was reduced to 5 nH from 7 nH in order to obtain a short rise-time current pulse, making the discharge-current road short by improving the arrangement of the current return plate,[6] as shown in the cross section of the laser chamber in Fig. 2. As a result, the energy efficiency for laser oscillation was enhanced.

Main discharge electrodes with narrow discharge width. The discharge width in the gas flow direction was reduced from 3.5 to 2.5 mm by improving the profile of the main discharge electrodes (their length: 640 mm) and their supporting system. Figure 3 shows the maximum repetition rate under arclike discharge free condition in the downstream region of gas flow (downstream arcing) as a function of an average gas velocity at the center of the discharge gap (gap length: 16 mm). In Fig. 3, the solid line shows the case of a 2.5 mm reduced discharge width and the dotted line shows

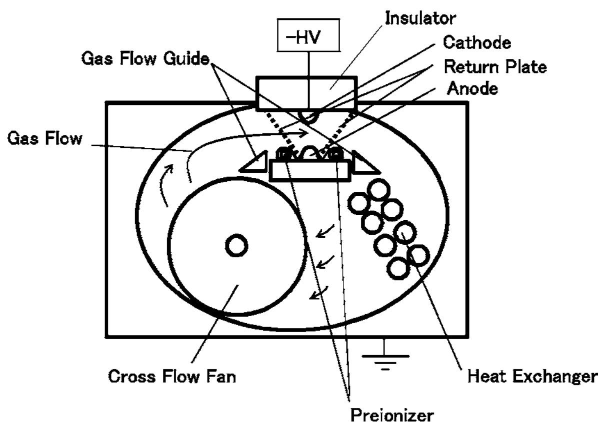

FIG. 2. Cross section of the laser chamber.

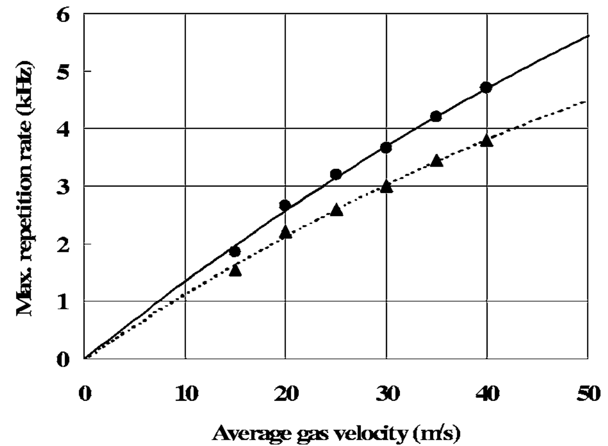

FIG. 3. Maximum repetition rate under downstream arcing free condition as a function of an average gas velocity. Discharge width of solid line: 2.5 mm and dashed line: 3.5 mm.

the case of a 3.5 mm discharge width. The results are shown in Secs. III B and III C.

A high-speed uniform gas-circulation system. One of the most important requirements for high-repetition-rate operation is the optimization of the gas flow condition in the discharge space. We developed a new gas-circulation system to provide a flow with high-average velocity and high uniformity at any position in the discharge space. The diameter of a cross flow fan is 150 mm. The heat exchanger was composed of eight water-cooling pipes. Furthermore, we designed gas flow guides to prevent gas flow on the anode and the cathode surfaces from decreasing, as shown in Fig. 2. In this system we did not use acoustic damper. The results are shown in Sec. III C.

A low-input power and high-intensity surface corona discharge preionizer. The preionizer electrodes were designed to provide a high-intensity homogeneous surface corona discharge by concentrating the electric field and increasing utilization rates of ultraviolet rays from a ladder electrode. The preionizer was composed of two cylindrical corona electrodes with an alumina dielectric tube between the inner electrode and outer electrode.[7] Consequently, the input power to the preionizer was reduced.

Reduction of impurity effect. Impurities in laser gases degrade ArF laser performance. We analyzed impurity effects on the laser performance. It was found that the addition of Xe gas (10 ppm) into the laser gas enhanced the preionization effect.[8] The Xe gas, which has low ionization potential, would mask possible contamination influences[9] and stabilize the laser performance.

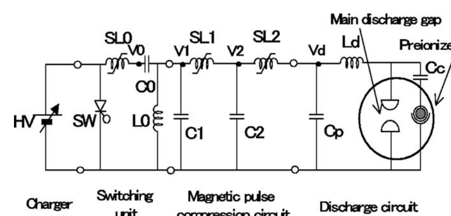

FIG. 4. Equivalent discharge circuit of ArF excimer laser.

Downloaded 08 May 2006 to 133.50.98.38. Redistribution subject to AIP license or copyright, see http://rsi.aip.org/rsi/copyright.jsp

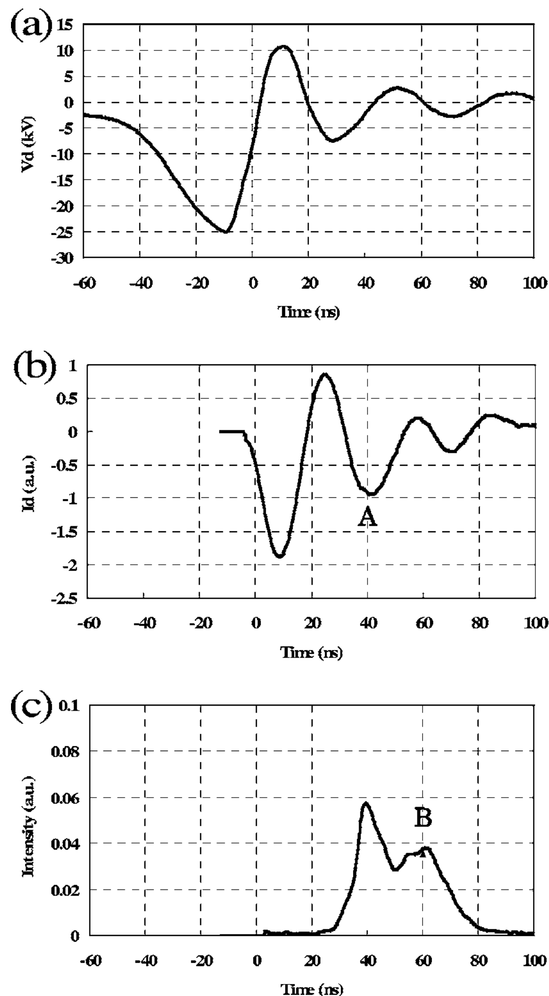

FIG. 5. Temporal wave forms of (a) voltage between the main discharge electrodes, (b) discharge current in the main discharge gap, and (c) laser pulse.

2. Pulse power module

A magnetic pulse compression (MPC) circuit with a high compression ratio. The rapidly rising voltage should be applied across the main electrodes so that the gas breakdown takes place by higher over voltage than the dc breakdown voltage. Then, this overvoltage breakdown provides high-density plasma, which may generate the needed excited state density to achieve useful laser gain. This speculation would be supported by that when the rise time is rapid, the breakdown voltage increases, and laser performance is improved.[10] Designing a lower residual inductance for the final stage of the MPC, we improved the SL2 structure and the MPC connection to the laser chamber. Then, the voltage rise time T_r across the main discharge electrodes was reduced to 50–60 ns from >100 ns.

A high-speed insulated gate bipolar transistor (IGBT) switching unit. We developed a new switching unit (SW) that is composed of several IGBTs for the pulse power module. The switching unit can be operated at repetition rates of up to 8 kHz.

B. Discharge circuit with long duration laser pulse

Figure 4 shows an excitation circuit of the ArF excimer laser. The discharge circuit is comprised of a two-stage magnetic pulse compression circuit using three magnetic switches SL0, SL1, and SL2. SL0 is used for the protection of solid-state switch SW. A two-stage magnetic pulse compression circuit is constructed from the first magnetic switch SL1 and second magnetic switch SL2. First, the voltage of a charger HV is adjusted to a prescribed level and main capacitor C0 is charged via SL0 and inductance L0. When C0 is completely charged, SW turns on. Then the charge in C0 transfers to capacitor C1. Subsequently, when the charge accumulated in C1 reaches the critical value determined by the characteristics of magnetic switch SL1, the magnetic flux in SL1 saturates and the SL1 turns on. Then, the current starts to flow in the loop circuit of C1, C2, and SL1. The charge accumulated in C1 transfers to C2. Here, the capacitances of C0, C1, and C2 are almost the same value.

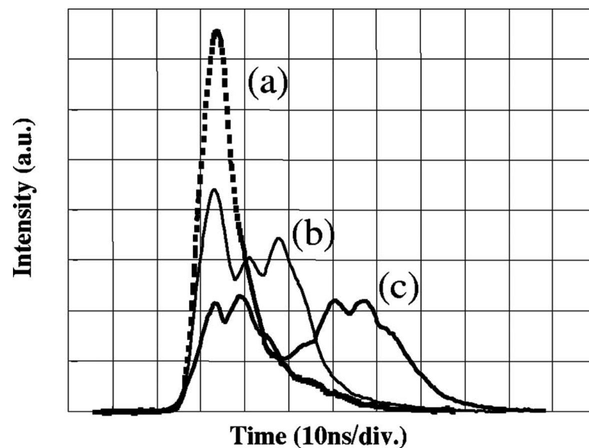

FIG. 6. Laser pulse wave form for (a) C_p/C2: 13.4/15.3 nF, T_r>100 ns (T_{is}=16 ns), (b) C_p/C2: 13.4/15.3 nF, T_r=50–60 ns (T_{is}=34 ns), and (c) C_p/C2: 9.0/15.3 nF, T_r=50–60 ns (T_{is}=50 ns).

When the charge accumulated in C2 reaches the critical value, current starts to flow in the loop circuit of C2, peaking capacitor C_p, and SL2. The corona discharge for preionization takes place on the outer peripheral surface of a dielectric tube, when the voltage between the main discharge electrodes V_d reaches the prescribed voltage. From corona discharge, ultraviolet rays are generated and simultaneously ionized Xe atoms are generated in the main discharge gap.

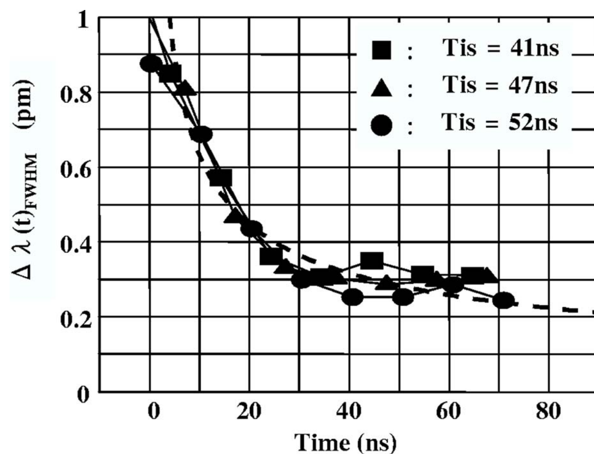

FIG. 7. Spectral bandwidth as a function of time.

Downloaded 08 May 2006 to 133.50.98.38. Redistribution subject to AIP license or copyright, see http://rsi.aip.org/rsi/copyright.jsp

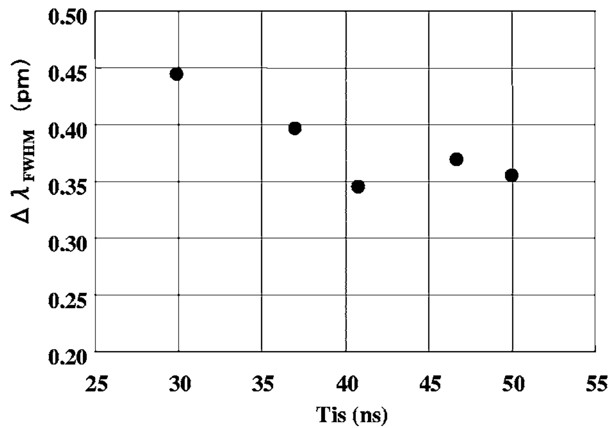

FIG. 8. Spectral bandwidth as a function of T_{is}.

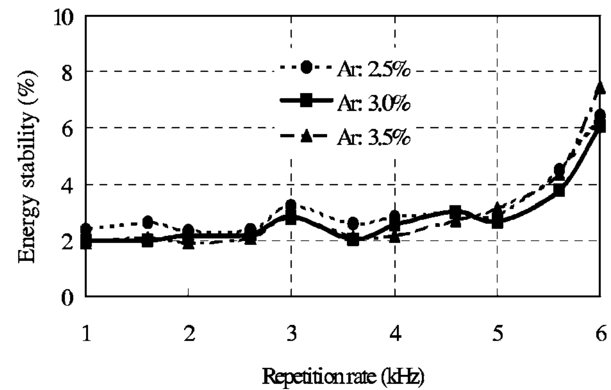

FIG. 10. Energy stability as a function of repetition rates for various Ar concentration ratios at a F_2 ratio of 0.09% and total pressure of 3 atm.

As C_p is charged further to the gas breakdown voltage V_d, the gap is broken down. The delay time between the main discharge and the corona discharge was about 35 ns. Figure 5 shows temporal wave forms of (a) a voltage between main discharge electrodes, (b) a discharge current in the main discharge gap, and (c) a laser pulse.

As the rise time of the primary current flowing through the main discharge gap is shortened, the peak current value is raised. It the same time, the main discharge continues in a stable manner. Then the charge remaining in C2, which brings the secondly current, is superimposed on the primary current [see (A) in Fig. 5(b)]. By doing so, the laser oscillation is brought by the first half-cycle of the discharge-current wave form and by at least following two half-cycles [see (B) in Fig. 5(c)]. As a result, the present system improved the discharge stability significantly, and accordingly the laser pulse duration stretched beyond 40 ns even when the system was operated at high repetition rates.

The fact shown above indicates that the present devices prevented spatial discharge constriction, which may occur in the latter half of the laser pulse.

III. EXPERIMENTAL RESULTS AND DISCUSSION

A. Laser pulse wave form and spectral bandwidth

Figure 6 shows laser pulse wave forms $P(t)$ in the narrow-bandwidth ArF excimer laser. The laser pulse duration varied according to the discharge circuit constant, $C_p/\mathrm{C2}$ and T_r. The pulse wave form (c) shows a full width at half maximum (FWHM) of about 45 ns and a time-integral-squared pulse width T_{is} of 50 ns. T_{is} is defined as follows:[11]

$$T_{is} = \left[\int P(t)dt \right]^2 \Big/ \int P(t)^2 dt. \quad (1)$$

The laser energy of all the pulses is 5 mJ.

The pulse with such long duration [see (c) in Fig. 6] can narrow the bandwidth by increasing the number of the round trips in a laser cavity equipped with the spectral bandwidth narrow module. Laser light passes through the spectral bandwidth narrow module every 7 ns because the laser cavity length is about 1 m. We obtained a convolved spectral bandwidth[12] with FWHM of about 0.60, 0.40, and 0.36 pm for T_{is} of 16, 34, and 50 ns, respectively.

Figure 7 shows the time evolution of spectral bandwidth $\Delta\lambda(t)_{\mathrm{FWHM}}$, which is measured through a grating monochromator equipped with a streak camera. The slit function, measured with an ultranarrowed solid-state laser, is 0.19 pm at FWHM.[13] We can see that the $\Delta\lambda(t)_{\mathrm{FWHM}}$ is independent of T_{is}. At the beginning of the laser pulse, $\Delta\lambda(t)_{\mathrm{FWHM}}$ is about 1.0 pm. After 30 ns passed, $\Delta\lambda(t)_{\mathrm{FWHM}}$ narrows to 0.35 pm. The dashed line was obtained by the following fitting equation:

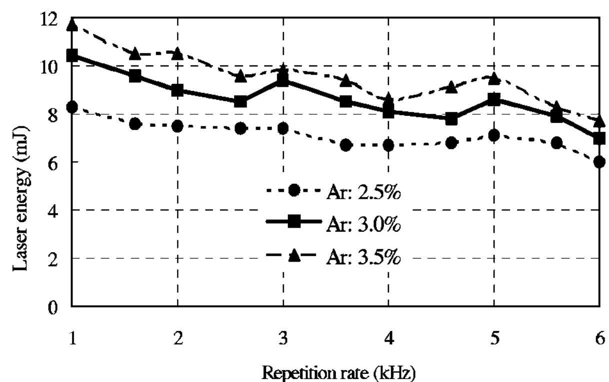

FIG. 9. Laser energy as a function of repetition rates for various Ar concentration ratios at a F_2 ratio of 0.09% and total pressure of 3 atm.

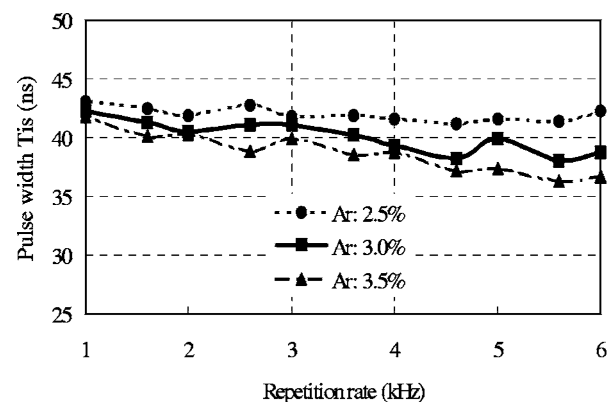

FIG. 11. Pulse width T_{is} as a function of repetition rates for various Ar concentration ratios at a F_2 ratio of 0.09% and total pressure of 3 atm.

Downloaded 08 May 2006 to 133.50.98.38. Redistribution subject to AIP license or copyright, see http://rsi.aip.org/rsi/copyright.jsp

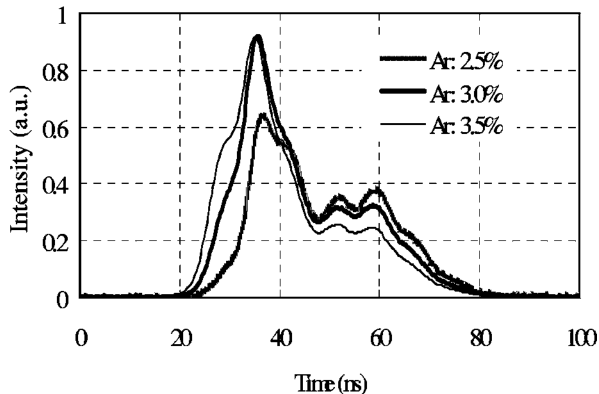

FIG. 12. Laser pulse wave form as a function of Ar concentration ratios at a F_2 ratio of 0.09% and total pressure of 3 atm.

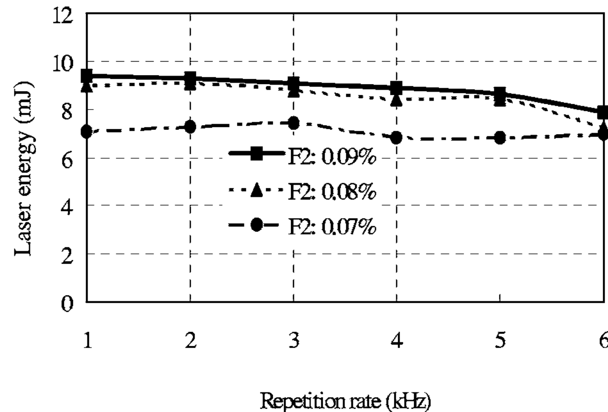

FIG. 14. Laser energy as a function of repetition rates for various F_2 concentration ratios at an Ar ratio of 3.0% and total pressure of 3 atm.

$$\Delta\lambda(t)_{\mathrm{FWHM}} = A/t^{1/2}(\mathrm{pm}), \quad A = 2. \tag{2}$$

We can see that $\Delta\lambda(t)_{\mathrm{FWHM}}$ is inversely proportional to the square root of time. The coefficient A depends on the resolution of the spectral bandwidth narrow module.

Figure 8 shows the time averaged $\Delta\lambda_{\mathrm{FWHM}}$ between 30 and 50 ns as a function of T_{is}. It shows that a longer T_{is} results in a narrower spectral bandwidth. We obtain $\Delta\lambda_{\mathrm{FWHM}}$ of 0.36 pm at T_{is} of 50 ns.

B. Laser characteristics after reducing the discharge width

The discharge width in the gas flow direction was reduced to 2.5 mm from 3.5 mm by improving the profile of the main discharge electrodes and their supporting system. As a result, the operating repetition rate increased to 5 kHz at 45 m/s, that is, the same gas velocity required for an operating repetition rate of 4 kHz at a 3.5 mm discharge width (see Fig. 2). The clearing ratio (CR) defined by the following equation may explain this result:[14]

$$\mathrm{CR} = \nu/(f_m\, w), \tag{3}$$

where υ is the interelectrode gas velocity, f_m is the maximum repetition rate under downstream arcing free condition, and w is the discharge width. Low gas velocity or wide discharge width operation causes downstream arcing that degrades energy stability. For the improved ArF excimer laser, f_m increased because CR is about 3.3.

Figures 9–11 show laser energy, pulse-to-pulse energy stability, and pulse width T_{is} as a function of the repetition rate, respectively. The Ar concentration ratios are varied at a F_2 ratio of 0.09% in a Ne buffer gas with a total pressure of 3 atm. The pulse-to-pulse energy stability (ES) is defined as follows:

$$\mathrm{ES} = (s/E_{\mathrm{ave}})100, \tag{4}$$

where s and E_{ave} are the standard deviation and the average laser energy for 500 pulses, respectively. For all the Ar concentration ratios, $\Delta\lambda_{\mathrm{FWHM}}$ was below 0.40 pm. In Fig. 9, we can see that the energy reductions against repetition rates as the Ar concentration ratio increases. Figure 10 shows that the energy stability deteriorates with decreasing the gas velocity due to the appearance of downstream arcing at repetition rates higher than 5 kHz. Figure 11 shows that the high Ar concentration ratio reduces the pulse width at higher repetition rates, though laser energy is high. In the 2.5% Ar concentration ratio, the pulse width was hardly reduced.

Figure 12 shows the laser pulse wave form for three Ar concentration ratios at a repetition rate of 6 kHz. As we can see, the latter half of the laser pulse decreased with increasing the Ar concentration ratio. Then a discharge constriction would occur in the latter half of the laser pulse.

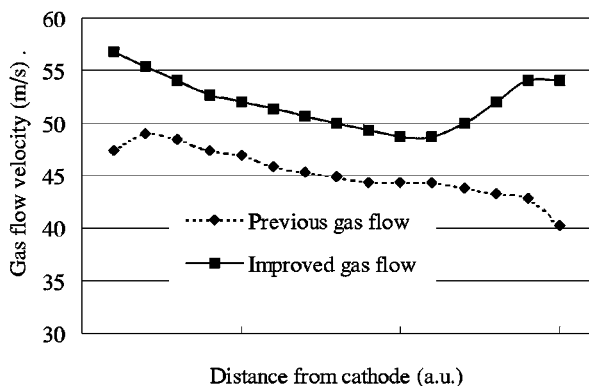

FIG. 13. Spatial distribution of time average gas flow velocity in discharge gap.

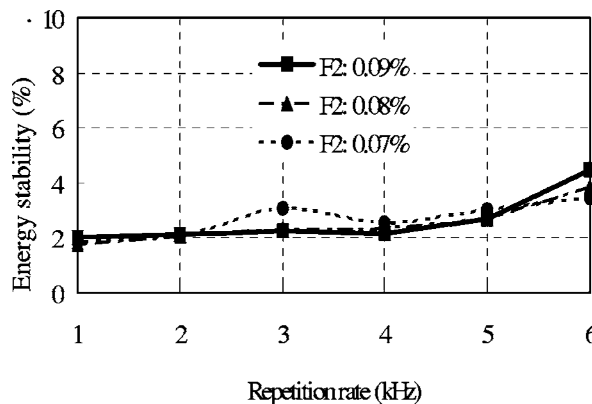

FIG. 15. Energy stability as a function of repetition rates for various F_2 concentration ratios at an Ar ratio of 3.0% and total pressure of 3 atm.

Downloaded 08 May 2006 to 133.50.98.38. Redistribution subject to AIP license or copyright, see http://rsi.aip.org/rsi/copyright.jsp

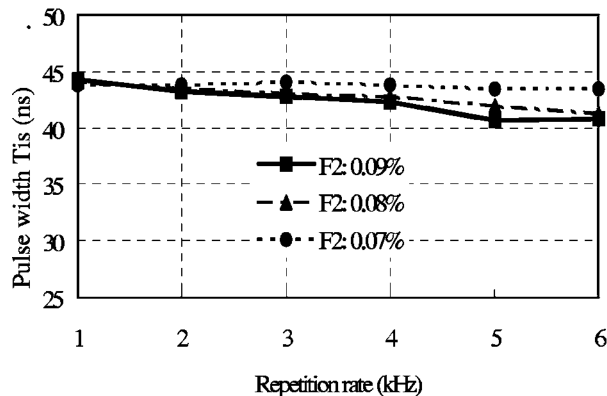

FIG. 16. Pulse width T_{is} as a function of repetition rates for various F_2 concentration ratios at an Ar ratio of 3.0% and total pressure of 3 atm.

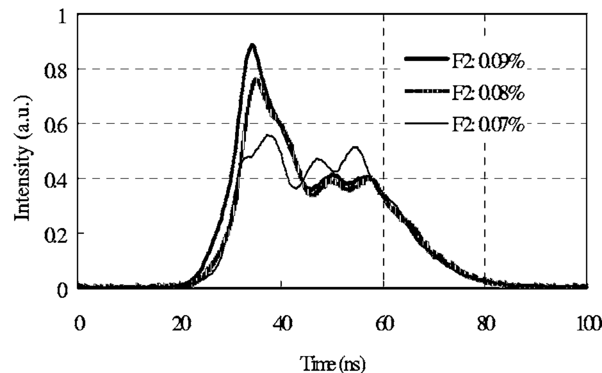

FIG. 17. Laser pulse shape as a function of F_2 concentration ratios at an Ar ratio of 3.0% and total pressure of 3 atm.

C. Laser characteristics after improving gas flow velocity and distribution

To improve the pulse-to-pulse energy stability at repetition rates over 5 kHz, we increased an average gas velocity to 50 m/s from 45 m/s at the center of the discharge gap. Furthermore, we designed a gas flow guide to prevent gas flow velocity on the anode and cathode surfaces from decreasing. Figure 13 shows the gas flow velocity distribution between the cathode and anode before and after the new gas flow guide was equipped. The vertical axis represents the gas flow velocity and the horizontal axis represents the distance from the cathode. As we can see, the gas flow on the electrode surfaces increased after the flow guide was equipped.

Figures 14–16 show laser energy, pulse-to-pulse energy stability, and pulse width T_{is} as a function of the repetition rate, respectively. The F_2 concentration ratios are varied at an Ar ratio of 3.0% in a Ne buffer gas and the total pressure is 3 atm. $\Delta\lambda_{FWHM}$ was below 0.40 pm in all the F_2 concentration ratios. Figure 14 shows that the laser energy reduction against repetition rates as the F_2 concentration ratios decrease. Figure 15 shows that the energy stability at 6 kHz improved to 4.5% from 6.0% in Fig. 10 due to improvement of the gas flow velocity and distribution (see Fig. 13). The energy stability at 6 kHz was improved to 3.5% from 4.5% with lowering the F_2 concentration ratio of 0.07% and then the laser energy reduction was small as shown in Fig. 14. Figure 16 shows that the pulse width was hardly reduced in the case of F_2 concentration ratio of 0.07% and then T_{is} of 44 ns is obtained at 6 kHz.

Figure 17 shows the laser pulse wave form at 6 kHz for the three cases of F_2 concentration ratios. The former half intensity of the laser pulse decreased, but the latter half intensity increased with decreasing the F_2 ratio.

[1] T. Saito *et al.*, Proc. SPIE **5377**, 1727 (2004).
[2] K. Kakizaki, T. Saito, K. Mitsuhashi, M. Arai, T. Tada, S. Kasahara, T. Igarashi, and K. Hotta, Proc. SPIE **4000**, 1397 (2000).
[3] J. Hueber *et al.*, Proc. SPIE **4000**, 1418 (2000).
[4] I. Bragin, V. Berger, P. Paetzel, U. Stamm, A. Targsdorf, J. Kleinschmidt, and D. Basting, Proc. SPIE **4000**, 1445 (2000).
[5] V. M. Borisov, A. I. Demin, A. V. Eltsov, O. B. Khristoforov, Y. B. Kiryukhin, A. V. ProkoFiev, A. Y. Vinokhodov, and V. A. Vodchits, Proc. SPIE **5137**, 241 (2002).
[6] K. Kakizaki and M. Arai, U.S. Patent No. 6,480,519 (12 November 2002).
[7] K. Kakizaki, K. Hotta, and M. Arai, U.S. Patent No. 6,654,402 (25 November 2003).
[8] N. Kataoka, T. Yabu, K. Uchino, K. Muraoka, T. Okada, E. Sunaka, T. Enami, and H. Mizoguchi, Trans. Inst. Electrical Eng. Jpn. **119-A**, 821 (1999).
[9] A. Sumitani *et al.*, Proc. SPIE **4000**, 1424 (2000).
[10] V. Osipov, Phys. Usp. **43**, 221 (2000).
[11] R. Sandstrom, Proceedings of the Second Symposium on 193 nm Lithography, Colorado Springs, CO, 1997 (unpublished) p. 17.
[12] P. A. Jansson, *Deconvolution of Images and Spectra*, 2nd ed. (Academic Press, New York, 1997), Chaps. 2–4.
[13] J. Sakuma, K. Deki, M. Horiguchi, T. Yokota, and T. Igarashi, Proceedings of the 60th Lecture by Applied Physics Group, 1999 (unpublished), 20-k-2, p. 930.
[14] G. Dzakowic and S. Wutzke, J. Appl. Phys. **44**, 5061 (1973).

Downloaded 08 May 2006 to 133.50.98.38. Redistribution subject to AIP license or copyright, see http://rsi.aip.org/rsi/copyright.jsp